In-motion Alignment for Low-cost SINS/GPS under Random Misalignment Angles

Xiao Cui[1], Chunbo Mei[2], Yongyuan Qin[1], Gongmin Yan[1] and Qiangwen Fu[1]

[1](*College of Automation, Northwestern Polytechnical University, China*)
[2](*No.203 Research Institute of China Ordnance Industries, China*)
(E-mail: cuixiao@mail.nwpu.edu.cn)

This paper presents a reliable in-motion alignment algorithm for a low cost Strapdown Inertial Navigation System/Global Positioning System (SINS/GPS) combination under random misalignment angles, which transforms attitude alignment into an attitude estimation problem. Based on Rodrigues parameters, an alignment model with a linear state-space equation and a second order nonlinear measurement equation is established. Furthermore, by employing a Taylor expansion on the nonlinear measurement equation, we implement a second order Extended Kalman Filter (EKF2). The proposed method uses a single filter that can not only determine the initial attitude, but also estimate the sensor errors. In addition, a scheme is given for avoiding singularity, which makes the algorithm more widely suitable for random misalignment angles. Experimental ground tests are performed with a low-cost Micro-Electromechanical System (MEMS) SINS, which validates the efficacy of the proposed method. The performance compared to the traditional alignment algorithm is also given.

1. INTRODUCTION.   The Inertial Navigation System (INS) is essentially a dead reckoning system. Hence, the initial condition, which is determined by the initial alignment, should be provided prior to navigation computation. Generally, the initial alignment for a high-precision INS can be achieved directly based on the output of gyros and accelerometers, known as self-alignment. For the low-cost INS, the noise threshold of gyros is near or higher than the Earth's rotation rate ($\approx 15°$/h), which means it cannot detect the Earth's rotation rate properly (Han and Wang, 2010). In this respect, the initial alignment approach for high-end INS is not feasible for low-cost INS. A popular approach is to use an external aiding sensor to provide additional information as reference for alignment.

With the vehicle held stationary, low cost systems initialise the pitch and roll angles using an accelerometer-measured gravitational field vector (Burak and Bekir, 2015). Heading is obtained externally using a magnetometer (Li and Wang, 2013). For systems integrated with the Global Positioning System (GPS), the velocity supplied by GPS provides a heading after the vehicle has started to move (Dissanayake et al., 2001). Unfortunately, the former method can only work effectively without dynamic accelerations and the measurements of magnetometers suffer from local magnetic interference. The latter method requires the vehicle to move at a strictly constant speed. In addition to this, the installation situation of INS relative to the vehicle should be determined prior to heading alignment.

The last decade has shown an increasing demand for small-sized and low-cost inertial navigation systems in many applications. However, initial alignment is still a challenging issue for these domains. It is especially difficult to estimate the attitude when the vehicle is moving. For example, smart munitions and guided missiles with a GPS-aided navigation system can be launched at any given time. The alignment must be done in-flight based on GPS information.

Various in-motion alignment techniques have been reported. Joon et al. (2004) suggested an in-flight alignment for a Strapdown Inertial Navigation System/Global Positioning System (SINS/GPS) using carrier phase rate measurement. The proposed method is more efficient than the velocity-aided one, which, nevertheless, requires two GPS antennae. Han and Wang (2010) introduced a two-stage Kalman filtering mechanism for the initial alignment of low-cost INS aided by GPS. The first stage is designed for the coarse alignment, and the second is for the fine alignment. Obviously, the alignment process must switch from a coarse alignment filter to a fine alignment filter. However, the error dynamic is just suitable for small attitude errors. To deal with large initial attitude error, some works provided nonlinear filtering methods (Scherzinger, 1996; Kong et al., 1999; Bimal and Ashok, 2015; Yuan et al., 2016). Kong et al. (1999) developed a non-linear error dynamics model for all three large misalignment angles. The benefit of this method is that the coarse alignment stage is eliminated. However, this model suffers from complex non-linear operations. Li et al. (2013) proposed a scheme for a Doppler Velocity Log (DVL)-aided Strapdown Inertial Navigation System (SINS) in-motion alignment using the Unscented Kalman Filter (UKF), which can deal with any initial heading errors. Bimal and Ashok (2015) developed a nonlinear wander azimuth error model that can be used for DVL-aided in-motion alignment and compared the performance of a UKF and an Extended Kalman Filter (EKF). This study did not consider sensor biases. The drawbacks of the above methods, however, are well-known linearization effects and computational load.

Recently, the Optimisation-Based initial Alignment (OBA) method has been developed (Gu et al., 2008; Silson, 2011; Wu et al., 2011; Kang et al., 2012; Li et al., 2014; Lu et al., 2016). The essence of the OBA method is to determine the constant attitude matrix at start-up of the initial alignment using infinite vector observations. Wu and Pan (2013) proposed an optimisation-based in-flight coarse alignment approach based on velocity/position integration. Flight tests of a navigation-grade SINS were used to evaluate the two alignment algorithms. However, they did not take the sensor bias into account and no test was done on low-cost SINS. Similar to Wu and Pan's method, Chang et al. (2015) extended the idea of the OBA method and gave a filtering called Modified Unscented Quaternion Estimator (MUSQUE) which can estimate the gyroscope biases other than the attitude quaternion.

In the present work, a Rodrigues parameters-based optimal estimator is proposed as a synthesis of the approaches mentioned above. Like the quaternion-based estimator, the proposed estimator consists of two stages. The first stage features an optimal estimation of a constant Rodrigues parameters vector. Then, the second stage produces a constant attitude matrix from the filtered Rodrigues parameters vector via the Cayley transform. Our contribution resides in the following properties:

- An ordinary linear Kalman Filter (KF) is applied on the state-space model. The measurement equation is quadratic with respect to the Rodrigues parameters vector. This equation is linearized by employing a Taylor expansion and the linearized model is implemented in a second order Extended Kalman Filter (EKF2), thus reducing the linearization effects of the EKF and avoiding the computational load of the nonlinear filter method.
- The initial alignment process does not need to be divided into two stages. A single Kalman Filter can complete the initial alignment under random misalignment angles.
- The proposed method circumvents one drawback of previous alignment methods, which is the difficulty of estimating parameters other than the attitude, such as the gyroscope and accelerometer biases. This is a desirable property for MEMS-based low-cost SINS.

The remainder of this paper is organised as follows. In Section 2, we review the conventional initial alignment scheme for low-cost SINS aided by GPS. In Section 3, based on Rodrigues parameters, the alignment dynamic model under random misalignment angles is established. Furthermore, employing exact Taylor series expansions, second-order EKF update equations are derived. Experimental tests on a vehicle with a low-cost MEMS Inertial Measurement Unit (IMU) are presented in Section 4. The data from dynamic experiments is processed by the proposed method and conventional in-motion initial alignment method for comparison. The conclusions of the present work are presented in the last section.

2. CONVENTIONAL INITIAL ALIGNMENT SCHEME FOR LOW-COST SINS AIDED BY GPS. The traditional initial alignment scheme aided by GPS is divided into two stages, namely, the coarse alignment stage and the fine alignment stage. The coarse alignment can be achieved through the classical least-squares approach generally introduced in 1965, the so-called Wahba's problem (Choukronun et al., 2004), which is a constrained least-squares estimation problem for finding the attitude matrix.

The fine alignment can be performed by a basic Kalman filter based on the INS linear error models of small attitude errors (Li et al., 2015; Han and Wang, 2010). Velocity and position information from the GPS with manoeuvring is employed as a measurement to estimate the residual attitude errors coming from the coarse alignment stage.

2.1. *Coarse Alignment in the Inertial Coordinate Frame.* It is easy to show that the apparent gravity expressed within the inertial space defines a cone whose main axis is the rotational axis of the earth, by using vector observations of the projective gravity vector to accomplish the initial Attitude Determination (AD), which transforms the attitude alignment into a constant attitude estimation problem.

The attitude matrix can be decomposed into three parts based on the chain rule as follows:

$$\boldsymbol{C}_b^n(t) = \boldsymbol{C}_{i_n}^n(t)\boldsymbol{C}_{i_b}^{i_n}\boldsymbol{C}_b^{i_b}(t) \tag{1}$$

where n and b are the local-level geographic frame and the body frame. i_n and i_b denote the auxiliary inertial frame, which are aligned with n and b at start-up of the alignment and are inertially "frozen" thereafter, respectively.

Equation (1) shows that the attitude matrix $\boldsymbol{C}_b^n(t)$ is composed of three parts:

(a) $\boldsymbol{C}_b^{i_b}(t)$ represents the time-varying attitude due to the rotation of the b-frame relative to the inertial frame i_b as a function of inertial angular rate which is measured by gyros

$$\dot{\boldsymbol{C}}_b^{i_b}(t) = \boldsymbol{C}_b^{i_b}(t)(\boldsymbol{\omega}_{ib}^b \times), \quad \boldsymbol{C}_b^{i_b}(t) = \boldsymbol{I} \tag{2}$$

using the two-sample coning correction algorithm (Savage, 1998; Qin, 2014).

The updating algorithm can be constructed as follows using the product chain rule:

$$\boldsymbol{C}_b^{i_b}(t_k) = \boldsymbol{C}_b^{i_b}(t_{k-1})\boldsymbol{C}_{b(t_k)}^{b(t_{k-1})} \tag{3}$$

(b) $\boldsymbol{C}_{i_n}^n(t)$ describes the time-varying attitude due to the earth rotation rate and the vehicle's transport rate relative to the Earth. The analytic expression is

$$\boldsymbol{C}_{i_n}^n(t) = \begin{bmatrix} \cos\delta\lambda & \sin L_0 \sin\delta\lambda & -\cos L_0 \sin\delta\lambda \\ -\sin L_k \sin\delta\lambda & \begin{pmatrix} \sin L_0 \sin L_k \cos\delta\lambda \\ +\cos L_0 \cos L_k \end{pmatrix} & \begin{pmatrix} -\sin L_k \cos L_0 \cos\delta\lambda \\ +\cos L_k \sin L_0 \end{pmatrix} \\ \cos L_k \sin\delta\lambda & \begin{pmatrix} -\sin L_0 \cos L_k \cos\delta\lambda \\ +\sin L_k \cos L_0 \end{pmatrix} & \begin{pmatrix} \cos L_0 \cos L_k \cos\delta\lambda \\ +\sin L_k \sin L_0 \end{pmatrix} \end{bmatrix} \tag{4}$$

where L_0 and λ_0 are the latitude and longitude at the start time of the alignment process; L_k and λ_k are the latitude and longitude at time t_k (output of GPS); $\delta\lambda = \lambda_k - \lambda_0 + \omega_{ie}t$.

(c) The core part $\boldsymbol{C}_{i_b}^{i_n}$ is a constant matrix, which represents the relationship between inertial frames i_b and i_n. According to Gu et al. (2008) and Wu and Pan (2013), $\boldsymbol{C}_{i_b}^{i_n}$ can be derived by solving the attitude determination problem using infinite vector observations as

$$\boldsymbol{V}^{i_n} = \boldsymbol{C}_{i_b}^{i_n}\boldsymbol{V}^{i_b} \tag{5}$$

where

$$\boldsymbol{V}^{i_b} = \int_0^t \boldsymbol{C}_b^{i_b}(t)\boldsymbol{f}^b(t)dt$$

$$\boldsymbol{V}^{i_n} = \int_0^t \boldsymbol{C}_n^{i_n}(t)\left[\dot{\boldsymbol{v}}^n + (2\boldsymbol{\omega}_{ie}^n + \boldsymbol{\omega}_{en}^n) \times \boldsymbol{v}^n - \boldsymbol{g}^n\right]\boldsymbol{f}^b(t)dt$$

Equation (5) is known as the classic Wahba's problem using two or more vector pair observations, and various authors (Choukronun et al., 2004) have presented solutions to this least squares optimisation problem. If the initial attitude matrix $\boldsymbol{C}_{i_b}^{i_n}$ is known, the continuous time $\boldsymbol{C}_b^n(t)$ can be obtained by Equation (1).

2.2. *Fine Alignment based on Kalman Filter.* The coarse alignment discussed in Section 2.1 will make the misalignment converge to a small angle. Under the condition of small platform misalignment, the fine alignment can proceed.

The state vector of the KF in the fine alignment process is generally selected as

$$X = \left[(\boldsymbol{\varphi}^n)^{\mathrm{T}} \quad (\delta \boldsymbol{v}^n)^{\mathrm{T}} \quad (\delta \boldsymbol{p}^n)^{\mathrm{T}} \quad \left(\boldsymbol{\varepsilon}^b\right)^{\mathrm{T}} \quad \left(\nabla^b\right)^{\mathrm{T}} \right]^{\mathrm{T}} \tag{6}$$

where $\boldsymbol{\varphi}^n$ denotes the misalignment angle, $\delta \boldsymbol{v}^n$ is the velocity error vector, and $\delta \boldsymbol{p}^n$ is the position error vector. $\boldsymbol{\varepsilon}^b$ and ∇^b denote the gyro and accelerometer biases, respectively.

Using navigation-frame GPS velocity and position aiding, the measurements used in the Kalman filter are the velocity and position differences between INS and GPS. Hence the measurement model is given below:

$$Z = \begin{bmatrix} \boldsymbol{v}^n_{INS} - \boldsymbol{v}^n_{GPS} \\ \boldsymbol{p}^n_{INS} - \boldsymbol{p}^n_{GPS} \end{bmatrix} = HX + V \tag{7}$$

where $H = \begin{bmatrix} \boldsymbol{0}_{6\times3} & \boldsymbol{I}_{6\times6} & \boldsymbol{0}_{6\times6} \end{bmatrix}$.

3. IN-MOTION ALIGNMENT FOR LOW-COST SINS/GPS AIDED BY GPS.

3.1. *Alignment Dynamic Model under Random Misalignment Angles.* Equation (5) cannot be satisfied by all the measurements, due to sensor noise. In particular, we assume that the integration of the accelerometer-measured specific force at time t_k in the inertial frame i_b is given by following expression:

$$\hat{\boldsymbol{V}}^{j_b}(t_k) = \boldsymbol{V}^{i_b}(t_k) + \delta \boldsymbol{V}^{i_b}(t_k) \tag{8}$$

where $\delta \boldsymbol{V}^{i_b}(t_k)$ is the integration error of $\boldsymbol{V}^{i_b}(t_k)$.

Then Equation (5) can be rewritten as

$$\boldsymbol{V}^{i_n}(t_k) = \boldsymbol{C}^{i_n}_{i_b} \left(\hat{\boldsymbol{V}}^{j_b}(t_k) - \delta \boldsymbol{V}^{i_b}(t_k) \right) \tag{9}$$

Our method is developed from the relationship equivalent to Equation (5), but written in terms of the Rodrigues vector. This is obtained by mapping the attitude matrix to a minimum-element attitude parameterisation expressed by the skew-symmetric Rodrigues matrix, using the Cayley transform (Daniele et al., 2007; Junkins and Kim, 1993). The relationship of attitude matrix $\boldsymbol{C}^{i_b}_{i_n}$ and the Rodrigues matrix is

$$\boldsymbol{C}^{i_b}_{i_n} = [\boldsymbol{I} + \boldsymbol{l}(\times)]^{-1} [\boldsymbol{I} - \boldsymbol{l}(\times)] \tag{10}$$

where $\boldsymbol{l}(\times)$ is a skew-symmetric matrix related to the elements of the Rodrigues vector $\boldsymbol{l}$.

Substituting Equation (10) into Equation (9) and reorganising the equation yields

$$\hat{\boldsymbol{V}}^{j_b}(t_k) = \boldsymbol{V}^{i_n}(t_k) = (\hat{\boldsymbol{V}}^{j_b}(t_k) + \boldsymbol{V}^{i_n}(t_k)) \times \boldsymbol{l} + \boldsymbol{l} \times \delta \boldsymbol{V}^{i_b}(t_k) + \delta \boldsymbol{V}^{i_b}(t_k) + \boldsymbol{w}_{t_k} \tag{11}$$

where $\boldsymbol{w}_{t_k}$ is the integration of the inertial sensor error.

Defining the sum and difference as follows:

$$\boldsymbol{S}_{t_k} = \hat{\boldsymbol{V}}^{j_b}(t_k) + \boldsymbol{V}^{i_n}(t_k), \quad \boldsymbol{D}_{t_k} = \hat{\boldsymbol{V}}^{j_b}(t_k) - \boldsymbol{V}^{i_n}(t_k) \tag{12}$$

Substituting Equation (12) into Equation (11), we obtain

$$\boldsymbol{D}_{t_k} = \boldsymbol{S}_{t_k} \times \boldsymbol{l} + \boldsymbol{l} \times \delta\boldsymbol{V}^{i_b}(t_k) + \delta\boldsymbol{V}^{i_b}(t_k) + \boldsymbol{w}_{t_k} \tag{13}$$

Equation (13) is the measurement equation of Rodrigues parameters vector $\boldsymbol{l}$, which is equivalent to constant attitude matrix $\boldsymbol{C}_{i_n}^{i_b}$. If the optimal estimate of Rodrigues parameters vector $\boldsymbol{l}$ is known, $\boldsymbol{C}_{i_n}^{i_b}$ can be obtained by Equation (10).

In Equation (2), we substitute $\boldsymbol{C}_b^{i_b}$, $\boldsymbol{\omega}_{i_b}^b$ by $\hat{\boldsymbol{C}}_b^{i_b}$ and $\hat{\boldsymbol{\omega}}_{i_b}^b$, respectively. The time subscripts are omitted for the sake of clarity, that is

$$\dot{\hat{\boldsymbol{C}}}_b^{i_b} = \hat{\boldsymbol{C}}_b^{i_b}(\hat{\boldsymbol{\omega}}_{i_b}^b \times) \tag{14}$$

assuming that the error of $\hat{\boldsymbol{C}}_b^{i_b}$ just introduced by gyro bias of SINS, and the computing platform misalignment angles $\boldsymbol{\varphi}^{i_b}$ is small in alignment process. Then we obtain

$$\hat{\boldsymbol{C}}_b^{i_b}(t) = \left[\boldsymbol{I}_3 - (\boldsymbol{\varphi}^{i_b} \times)\right] \boldsymbol{C}_b^{i_b} \tag{15}$$

$$\hat{\boldsymbol{\omega}}_{i_b}^b = \boldsymbol{\omega}_{i_b}^b + \boldsymbol{\varepsilon}^b + \boldsymbol{w}_g^b \tag{16}$$

where $\boldsymbol{\varepsilon}^b$, $\boldsymbol{w}_g^b$ are gyro biases and the noise of SINS, respectively.

Now if we can differentiate both sides of Equation (15) and substitute Equations (2), (14) and (16) then we obtain the following differential equation

$$\dot{\boldsymbol{\varphi}}^{i_b} = -\hat{\boldsymbol{C}}_b^{i_b}(\boldsymbol{\varepsilon}^b + \boldsymbol{w}_g^b), \boldsymbol{\varphi}^{i_b}(0) = 0 \tag{17}$$

From Equations (5) and (8) we can see that

$$\hat{\boldsymbol{V}}^{j_b} = \boldsymbol{V}^{i_b} + \delta\boldsymbol{V}^{i_b} = \int_0^t \hat{\boldsymbol{C}}_b^{i_b}\hat{\boldsymbol{f}}^b \, dt \tag{18}$$

$$\hat{\boldsymbol{f}}^b = \boldsymbol{f}^b + \nabla^b + \boldsymbol{w}_a^b \tag{19}$$

where $\nabla^b, \boldsymbol{w}_a^b$ are accelerometer biases and the noise of SINS, respectively.

Substituting Equations (15) and (19) into Equation (18), and discarding the higher order slim terms, we have

$$\delta\dot{\boldsymbol{V}}^{i_b} = \hat{\boldsymbol{f}}^{i_b} \times \boldsymbol{\varphi}^{i_b} + \hat{\boldsymbol{C}}_b^{i_b}(\nabla^b + \boldsymbol{w}_a^b), \delta\boldsymbol{V}^{i_b}(0) = 0 \tag{20}$$

As the matrix $\boldsymbol{C}_{i_n}^{i_b}$ can be considered as a constant attitude matrix during the alignment process, the correlated Rodrigues parameters vector in Equation (10) satisfies the following differential equation

$$\boldsymbol{l} = \boldsymbol{0} \tag{21}$$

Equations (17), (20), and (21) constitute the dynamic model. Taking the gyroscope drifts $\boldsymbol{\varepsilon}^b$ and accelerometer biases ∇^b into account as constant, the complete state vector is

selected as follows

$$X = \begin{bmatrix} l^{\mathrm{T}} & \left(\boldsymbol{\varphi}^{i_b}\right)^{\mathrm{T}} & \left(\delta \boldsymbol{V}^{i_b}\right)^{\mathrm{T}} & \left(\boldsymbol{\varepsilon}^b\right)^{\mathrm{T}} & \left(\nabla^b\right)^{\mathrm{T}} \end{bmatrix}^{\mathrm{T}} \qquad (22)$$

The alignment dynamic model under random misalignment angles can therefore be written as

$$\begin{bmatrix} \dot{l} \\ \dot{\boldsymbol{\varphi}}^{i_b} \\ \delta \dot{\boldsymbol{V}}^{i_b} \\ \dot{\boldsymbol{\varepsilon}}^b \\ \dot{\nabla}^b \end{bmatrix} = \begin{bmatrix} \boldsymbol{0}_{3\times3} & \boldsymbol{0}_{3\times3} & \boldsymbol{0}_{3\times3} & \boldsymbol{0}_{3\times3} & \boldsymbol{0}_{3\times3} \\ \boldsymbol{0}_{3\times3} & \boldsymbol{0}_{3\times3} & \boldsymbol{0}_{3\times3} & -\hat{\boldsymbol{C}}_b^{i_b} & \boldsymbol{0}_{3\times3} \\ \boldsymbol{0}_{3\times3} & \hat{\boldsymbol{f}}^{i_b}\times & \boldsymbol{0}_{3\times3} & \boldsymbol{0}_{3\times3} & \hat{\boldsymbol{C}}_b^{i_b} \\ \boldsymbol{0}_{3\times3} & \boldsymbol{0}_{3\times3} & \boldsymbol{0}_{3\times3} & \boldsymbol{0}_{3\times3} & \boldsymbol{0}_{3\times3} \\ \boldsymbol{0}_{3\times3} & \boldsymbol{0}_{3\times3} & \boldsymbol{0}_{3\times3} & \boldsymbol{0}_{3\times3} & \boldsymbol{0}_{3\times3} \end{bmatrix} \begin{bmatrix} l \\ \dot{\boldsymbol{\varphi}}^{i_b} \\ \delta \boldsymbol{V}^{i_b} \\ \boldsymbol{\varepsilon}^b \\ \nabla^b \end{bmatrix} + \begin{bmatrix} \boldsymbol{0}_{3\times1} \\ -\hat{\boldsymbol{C}}_b^{i_b}\boldsymbol{w}_g \\ \hat{\boldsymbol{C}}_b^{i_b}\boldsymbol{w}_a \\ \boldsymbol{0}_{3\times1} \\ \boldsymbol{0}_{3\times1} \end{bmatrix} \qquad (23)$$

Equation (13) can be rewritten as

$$\boldsymbol{Z}_k = \boldsymbol{D}_k = h(X_k) + \boldsymbol{w}_k = \boldsymbol{S}_k \times l + (\boldsymbol{I} + l\times)\delta \boldsymbol{V}^{i_b} + \boldsymbol{w}_k \qquad (24)$$

Note that the measurement Equation (24) is derived without any assumption for misalignment, which means that the alignment dynamic model can be established in the same form whether the misalignment angle is small or not. In this respect, a unified in-motion alignment model under random misalignment angles is proposed based on integration of the specific force.

3.2. *Second-order Nonlinear Measurement Filter Algorithm based on Second-order Extended Kalman Filter.* The state process Equation (23) is linear. In contrast, the measurement Equation (24) is quadratic nonlinear. Measurement Equation (24) is linearized accurately by applying a Taylor series expansion around X_{k0} to second-order terms as

$$h(X_k) = h(X_{k0}) + \boldsymbol{H}_k X_k + \frac{1}{2}\sum_{i=1}^{3} \boldsymbol{e}_i \mathrm{Tr}(\boldsymbol{D}_i \tilde{X}_k \tilde{X}_k^{\mathrm{T}}) \qquad (25)$$

where X_{k0} is the current best estimate of X_k, $\tilde{X}_k = X_k - X_{k0}$, $\boldsymbol{e}_i$ is a 3×1 unit vector with 1 in the element i and 0 elsewhere, $\boldsymbol{H}_k$ denotes the Jacobian matrix of the nonlinear function h, $\boldsymbol{D}_i$ denotes the Hessian matrix of the nonlinear function h, and "Tr" denotes the trace operator.

Note that the second partial derivative matrix of nonlinear function is a constant matrix. That is, the element of matrix $\boldsymbol{D}_i$ is scalar. From Equations (23) and (24), nonzero scalars of $\boldsymbol{D}_i$ are as follows:

$$\begin{aligned} \boldsymbol{D}_1(2,9) = 1, && \boldsymbol{D}_2(1,9) = -1, && \boldsymbol{D}_3(1,8) = 1, \\ \boldsymbol{D}_1(3,8) = -1, && \boldsymbol{D}_2(3,7) = 1, && \boldsymbol{D}_3(2,7) = -1, \\ \boldsymbol{D}_1(9,2) = 1, && \boldsymbol{D}_2(9,1) = -1, && \boldsymbol{D}_3(8,1) = 1, \\ \boldsymbol{D}_1(8,3) = -1, && \boldsymbol{D}_2(7,3) = 1, && \boldsymbol{D}_3(7,2) = -1, \end{aligned} \qquad (26)$$

The remaining elements in matrix $\boldsymbol{D}_i$ are zeros.

Equation (23) is clearly a linear state equation. This means we can use the standard KF equations to estimate the state.

Now we will derive the measurement update equations based on Equation (25) in the form of a second-order Taylor series expansion. Suppose that the state estimate at t_k is given as

$$\hat{X}_k = \hat{X}_{k/k-1} + K_k \left[Z_k - h(\hat{X}_{k/k-1}) - L_k \right] \tag{27}$$

where L_k is a correction term to assure the estimate $\hat{X}_k$ is unbiased, and we will then choose K_k to minimise the trace of the covariance of the estimate.

Define the estimate errors as

$$\tilde{X}_k = X_k - \hat{X}_k = \hat{X}_{k/k-1} - (\hat{X}_k - \hat{X}_{k-1}) \tag{28}$$

where $\tilde{X}_{k/k-1} = X_k - \hat{X}_{k/k-1}$

From Equations (25), (27) and (28), we have

$$\tilde{X}_k = \tilde{X}_{k/k-1} - K_k H_k \tilde{X}_{k/k-1} - K_k w_k - K_k \left[\frac{1}{2} \sum_{i=1}^{3} e_i \mathrm{Tr}(D_i \tilde{X}_{k/k-1} \tilde{X}_{k/k-1}^{\mathrm{T}}) - L_k \right] \tag{29}$$

Assuming that time-update $\hat{X}_{k/k-1}$ is unbiased, taking the expected value of both sides of Equation (29) and making the result zeros, we obtain

$$L_k = E \left[\frac{1}{2} \sum_{i=1}^{3} e_i \mathrm{Tr}(D_i \tilde{X}_{k/k-1} \tilde{X}_{k/k-1}^{\mathrm{T}}) \right] = \frac{1}{2} \sum_{i=1}^{3} e_i \mathrm{Tr}(D_i P_{k/k-1}) \tag{30}$$

Substituting Equation (30) into Equation (29) we have

$$\tilde{X}_k = (I - K_k H_k) \tilde{X}_{k/k-1} + K_k A - K_k w_k \tag{31}$$

where

$$A = \frac{1}{2} \sum_{i=1}^{3} e_i \mathrm{Tr} \left[(D_i P_{k/k-1})(D_j P_{k/k-1}) \right] \tag{32}$$

Since $E(\tilde{X}_k) = 0, E(w_k) = 0$, w_k and A are uncorrelated, we can see from Equations (31) and (32) that

$$P_k = E \left[\tilde{X}_k \tilde{X}_k^{\mathrm{T}} \right] = (I - K_k H_k) P_{k/k-1} (I - K_k H_k)^{\mathrm{T}} + K_k (R_k + \Lambda_k) K^{\mathrm{T}} \tag{33}$$

where

$$\Lambda_k = E \left[A A^{\mathrm{T}} \right] \tag{34}$$

The second-order EKF can be summarised in the following. Additional derivations can be found in Simon (2006) or Qin et al. (2014).

a) Time-update equations:

$$\hat{X}_{k/k-1} = \Phi_{k/k-1} \hat{X}_{k-1} \tag{35}$$

$$P_{k/k-1} = \Phi_{k/k-1} P_{k-1} \Phi_{k/k-1}^{\mathrm{T}} + Q_k \tag{36}$$

b) Measurement update equations:

$$\hat{X}_k = \hat{X}_{k/k-1} + K_k \left[Z_k - h(\hat{X}_{k/k-1}) - L_k \right] \tag{37}$$

$$K_k = P_{k/k-1} H_k^{\mathrm{T}} (H_k P_{k/k-1} H_k^{\mathrm{T}} + R_k + \Lambda_k)^{-1} \tag{38}$$

$$\Lambda_k(i,j) = \frac{1}{2} \mathrm{Tr} \left[(D_i P_{k/k-1})(D_j P_{k/k-1}) \right] \tag{39}$$

$$P_k = (I - K_k H_k) P_{k/k-1} (I - K_k H_k)^{\mathrm{T}} + K_k (R_k + \Lambda_k) K^{\mathrm{T}} \tag{40}$$

From Measurement update Equations (35)∼(40), we know that the second-order EKF equations are similar to the conventional linear KF, just with two additional terms, L_k and Λ_k.

3.3. *Scheme for Avoiding Singularity.* The well-known Rodrigues parameters algorithm suffers from a singularity in the case of a π-rotation between the coordinate frames, i_b and i_n, because the norm of the Gibbs vector becomes unbounded for such a rotation (Qin et al., 2014; Mei et al., 2015). This problem can be eliminated completely by employing the method of sequential rotations, as introduced in Shuster and Oh (1980). We apply a certain virtual rotation from the frame i_b to a new coordinate frame $i_{b'}$, and make the Rodrigues parameters that represent the orientation of $i_{b'}$ and i_n away from the singular position. By so doing, the estimation of $l_{i_n}^{i_b}$ can also be obtained indirectly from the result $l_{i_n}^{i_{b'}}$, which is the basic idea of designing the scheme for avoiding singularity.

However, in practice, it is possible to know in advance which rotation is not needed due to the principal axis being far from its singular position (Daniele et al., 2007). For example, in the Rodrigues parameters algorithm singularity for land vehicles or airborne vehicles, which occurs only when the attitude angles are small, the yaw angle is close to π (Mei et al., 2015). Then, the singularity avoiding method of GPS-aiding is summarised below.

Step 1: At the start-up of the alignment, the estimate of yaw angle and pitch angle are available by using only the GPS velocity measurement vector $\hat{v}_0^n$

$$\begin{cases} \hat{\psi} = \arctan 2(\hat{v}_{0E}^n, \hat{v}_{0N}^n) \\ \hat{\theta} = \arctan 2 \left(\hat{v}_{0U}^n, \sqrt{\left(\hat{v}_{0E}^n\right)^2 + \left(\hat{v}_{0N}^n\right)^2} \right) \end{cases} \tag{41}$$

where $\arctan 2$ is the four-quadrant tangent inverse, $\hat{v}_{0i}^n (i = E, N, U)$ are the GPS velocity measurement components in the East, North and vertical direction, respectively.

Step 2: Compute the projected components of specific force in the inertial frame using the GPS velocity outputs $\hat{v}_1^n$ at 1s (the sample period for GPS is 1 s) and $\hat{v}_0^n$

$$\hat{f}^n = (\hat{v}_1^n - \hat{v}_0^n) + (2\omega_{ie}^n + \omega_{en}^n) \times \frac{\hat{v}_1^n + \hat{v}_0^n}{2} - g^n \tag{42}$$

Step 3: We define a frame as a rotation sequence: the frame must be rotated by $-\psi$ around its z-axis and then by θ about its x-axis. Therefore, we can obtain the transformation

from the n''-frame to the n-frame using the result of Step 1

$$\hat{\boldsymbol{C}}_n^{n''}(\hat{\psi}, \hat{\theta}) = \begin{bmatrix} 1 & 0 & 0 \\ 0 & \cos\hat{\theta} & \sin\hat{\theta} \\ 0 & \sin\hat{\theta} & \cos\hat{\theta} \end{bmatrix} \begin{bmatrix} \cos\hat{\psi} & -\sin\hat{\psi} & 0 \\ \sin\hat{\psi} & \cos\hat{\psi} & 0 \\ 0 & 0 & 1 \end{bmatrix} \tag{43}$$

Then, we use the computed attitude matrix $\hat{\boldsymbol{C}}_n^{n''}(\hat{\psi}, \hat{\theta})$ to project $\hat{\boldsymbol{f}}^n$ into the n''-frame

$$\hat{\boldsymbol{f}}^{n''} = \hat{\boldsymbol{C}}_n^{n''}(\hat{\psi}, \hat{\theta})\hat{\boldsymbol{f}}^n \tag{44}$$

Step 4: Compute the mean of the specific force in inertial b-frame using the accelerometer outputs over 1 s

$$\hat{\bar{\boldsymbol{f}}}^b = \frac{1}{N}\sum_{k=1}^{N}\hat{\boldsymbol{f}}^b(t_k), t_k \in [0, 1] \tag{45}$$

where t_k is the current sample time, $t_k = k \cdot t_s (k = 0, 1, \cdots N)$, where the sample period is t_s.

Step 5: From the former definition of the n''-frame, we see that the transformation matrix from the n''-frame to the b-frame corresponds to the elementary matrix only with an angle γ, so the results of $\hat{\bar{\boldsymbol{f}}}^{n''}$ and $\hat{\bar{\boldsymbol{f}}}^b$ in Step 3 and Step 4 can be used to estimate the roll angle.

$$\hat{\gamma} = \arctan 2\left(\hat{\bar{f}}_z^b\hat{f}_x^{n''} - \hat{\bar{f}}_x^b\hat{f}_z^{n''}, \ \hat{\bar{f}}_x^b\hat{f}_x^{n''} + \hat{\bar{f}}_z^b\hat{f}_z^{n''}\right) \tag{46}$$

where $\hat{\bar{f}}_x^b, \hat{\bar{f}}_z^b$, are the first and third components of $\hat{\bar{\boldsymbol{f}}}^b$, respectively; $\hat{f}_x^{n''}, \hat{f}_z^{n''}$ are the first and third components of $\hat{\bar{\boldsymbol{f}}}^{n''}$, respectively.

Step 6: we denote an attitude matrix $\boldsymbol{C}_{i_b}^{i_{b'}}$ computed using the estimates, $\hat{\psi}, \hat{\theta}$ and $\hat{\gamma}$, as the virtual rotation, which indicates the transformation from the frame i_b to a new coordinate frame $i_{b'}$.

Furthermore, the necessity of determining the Rodrigues parameters vector $\boldsymbol{l}_{i_n}^{i_{b'}}$ must be resolved though the $\boldsymbol{C}_{i_b}^{i_{b'}}$ to obtain the vector observations in the $i_{b'}$-frame. That is, the corresponding vectors in the i_b-frame should be transformed into the $i_{b'}$-frame by $\boldsymbol{C}_{i_b}^{i_{b'}}$.

When the $\boldsymbol{C}_{i_n}^{i_{b'}}$ can be obtained by Equation (10), the $\boldsymbol{C}_{i_n}^{i_b}$ is

$$\boldsymbol{C}_{i_n}^{i_b} = (\boldsymbol{C}_{i_b}^{i_{b'}})^{\mathrm{T}} \cdot \boldsymbol{C}_{i_n}^{i_{b'}} \tag{47}$$

Steps 1~6 introduce a scheme for avoiding singularity, which occurs when the attitude angles are small, and the yaw angle is close to π.

4. ALIGNMENT EXPERIMENTAL TEST ON A VEHICLE.   In this section, road test experiments in a land vehicle are carried out to validate and corroborate the performance of the proposed algorithm with a focus on the comparison with the traditional in-motion initial alignment method. The experimental platform is shown in Figure 1, which is composed of a MEMS Inertial Measurement Unit (MIMU, Stim-300 from the Sensonor company), GPS and a POS (Position and Orientation System, POS) system (LV-610 from the Applanix company). The POS system is a type of high-accuracy integrated navigation system. Here

Figure 1. Setup of the experimental platform.

Table 1. Specifications of the Stim-300.

	Gyroscope	Accelerometer
Dynamic range	$\pm 400^\circ/s$	$\pm 10\,g$
Update rate	100 Hz	100 Hz
Bias	$-250^\circ/h \sim +250^\circ/h$	$-0{\cdot}75$ mg $\sim +0{\cdot}75$ mg
Bias stability	$0{\cdot}5^\circ/h$(Allan)	$0{\cdot}05$ mg(Allan)
Random Walk	$0{\cdot}15^\circ/\sqrt{h}$(Allan)	$0{\cdot}06\,m/s/\sqrt{h}$(Allan)

Table 2. Accuracy Specifications of the POS LV-610(PP).

	With GPS	GPS Outage (1 km or one minute)
Roll and Pitch ($^\circ$)	0·005	0·005
Heading ($^\circ$)	0·15	0·15
X,Y Position (m)	0·02	0·1
Z Position (m)	0·05	0·07

it is used to provide the reference attitude with high accuracy for initial alignment performance comparison. The specifications of the MIMU and the accuracy specifications of the POS are listed in Tables 1 and 2, respectively.

It is known that the yaw misalignment angle is not observable without horizontal accelerations. Based on attitude estimation using the vector observations algorithm, we know that all possible constraint manoeuvres should be performed to change the acceleration to change the direction of the integration vector. Therefore, after beginning alignment, the vehicle should accelerate in a straight line or make turning manoeuvres as a necessary condition for in-motion alignment. The reference yaw and velocity during the test are shown in Figure 2.

In the experiment, the initial state covariance matrix $\boldsymbol{P}_0$ has diagonal entities of the corresponding state variances. The proposed method and the conventional fine alignment
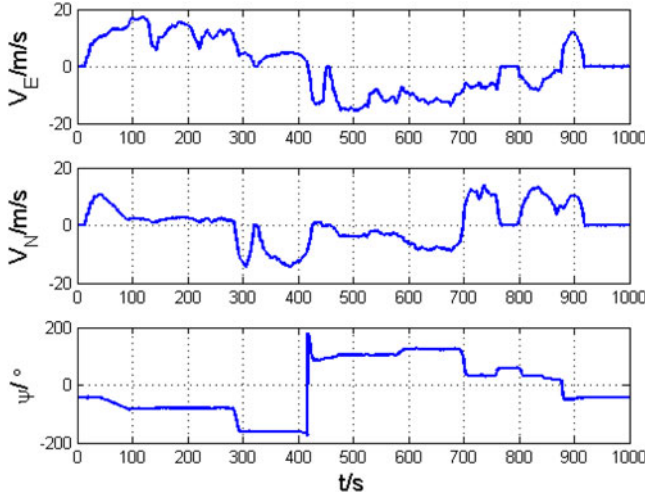
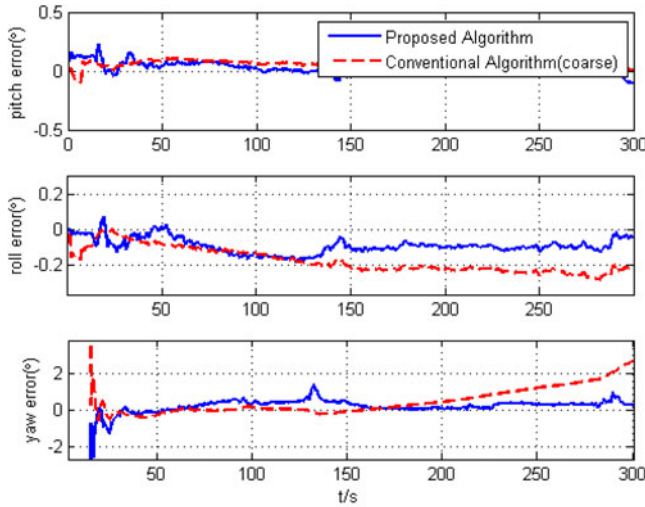Figure 2.   Velocity and yaw during the test.

Figure 3.   Alignment errors comparison between the proposed method and conventional coarse alignment.

are set as follows

$$\begin{cases} P_0 = diag([P_l, P_{\varphi^{ib}}, P_{\delta V^{ib}}, P_\varepsilon, P_\nabla]), (proposed\ method) \\ P_0 = diag([P_\phi, P_{\delta v}, P_{\delta p}, P_\varepsilon, P_\nabla]), (conventional\ method) \end{cases}$$

where $P_{l_j} = (1)^2$, $P_{\varphi_j^{ib}} = (1e-4')^2$, $P_{\delta V_j^{ib}} = (0{\cdot}1\text{m/s})^2$, $P_{\phi_j} = (1°)^2$, $P_{\delta v_j} = (0{\cdot}1\text{m/s})^2$, $P_{\delta P} = (10\text{m})^2$, $P_{\varepsilon_j} = (100°/\text{h})^2$, $P_{\nabla_j} = (3\text{mg})^2$.

The two methods have the same measurement noise covariance matrix $R = diag([0{\cdot}1\quad 0{\cdot}1\quad 0{\cdot}1]^2)$ and this is chosen based on the GPS output uncertainties. The Q matrix is created using the inertial sensors' noise statistics shown in Table 1.
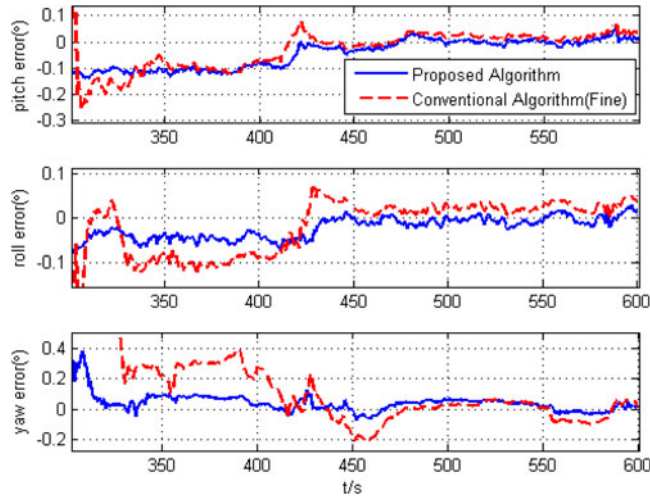
Figure 4.   Alignment errors comparison between the proposed method and conventional fine alignment.
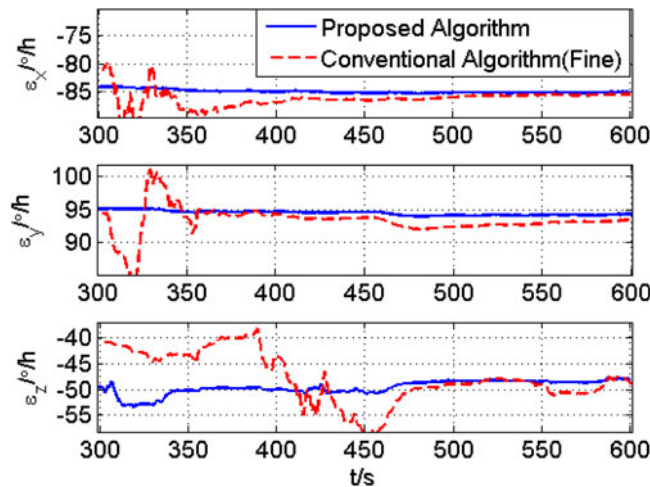

Figure 5.   Gyroscope biases estimation.

The results of our method and conventional alignment algorithm are compared to the reference POS system. Figures 3 and 4 illustrate the alignment error in the alignment process. Figure 3 shows the alignment error from 0 s to 300 s to compare the proposed method with conventional coarse alignment, while Figure 4 compares results of our method and conventional fine alignment from 300 s to 600 s.

It is shown that the alignment performance of the proposed approach has obvious improvements compared with that of the conventional approach. In particular, the yaw estimation converges much faster and achieves higher accuracy than that of the more conventional algorithm. The results indicate that the heading could reach around 0·1° accuracy and the pitch and roll could be aligned up to 0·05° during the alignment.
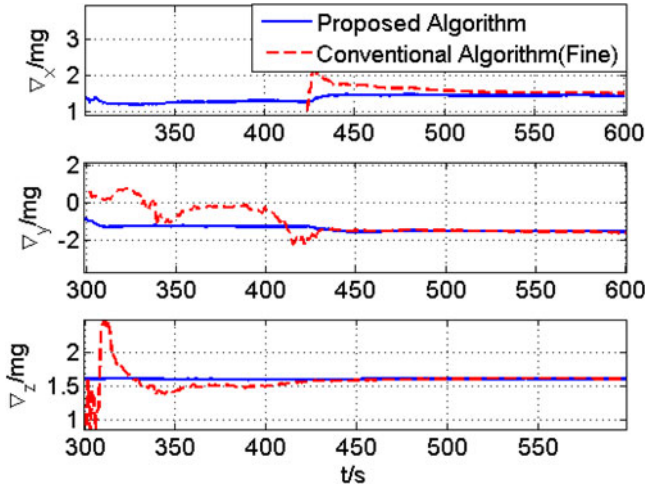
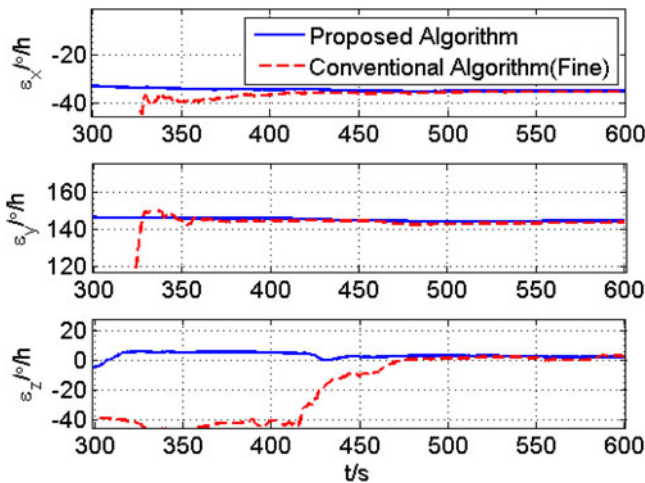Figure 6.   Accelerometer biases estimation.

Figure 7.   Gyroscope biases estimation (unknown true constant + 50°/h).

The gyroscope and accelerometer bias estimates are shown in Figures 5 and 6, respectively. Since the sensor biases have a dominating effect on the performance of initial alignment, especially for the low-cost SINS, a better knowledge of the sensor biases yields a more accurate attitude estimate. This is why the proposed approach has superior performance over the conventional algorithm. In addition, we have added 50°/h and 5 mg biases into the outputs of gyroscopes and accelerometers, respectively. We can compare the bias estimation accuracy indirectly by the biases estimation results before and after the addition. Figures 7 and 8 show the estimation results of biases after the addition, and the estimation results at the final time of alignment are summarised in Table 3.

It is seen that the proposed approach provides a slight improvement in estimation accuracy over the classical fine alignment by comparing the bias estimation results
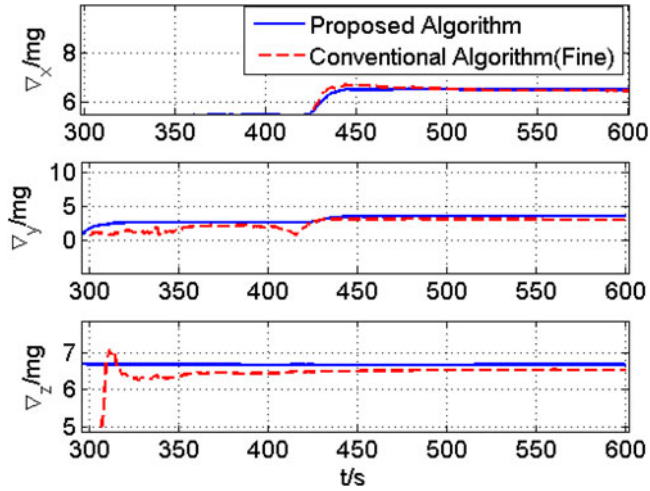
Figure 8. Accelerometer biases estimation (unknown true constant + 5 mg).

Table 3. Gyroscope and Accelerometer biases estimation results.

Bias	Value	Classical Fine Alignment	Proposed Approach
Gyro	unknown true constant	−85·4848	−85·1443
		93·4871	94·3245
		−48·8330	−48·0853
	unknown true constant + 50°/h	−35·2789	−35·1794
		143·7221	144·3871
		1·9972	1·9868
Acc	unknown true constant	1·5169	1·4461
		−1·5948	−1·5145
		1·6033	1·6011
	unknown true constant + 5 mg	6·4521	6·5052
		2·9294	3·4680
		6·5199	6·6652

before and after the addition. The former can reach $[49 \cdot 9649 \quad 50 \cdot 0626 \quad 50 \cdot 0721]^{\mathrm{T}\circ}/\mathrm{h}$ and $[5 \cdot 0591 \quad 4 \cdot 9825 \quad 5 \cdot 0641]^{\mathrm{T}}$ mg respectively, whereas the latter is $[50 \cdot 2059 \quad 50 \cdot 2350 \quad 50 \cdot 8302]^{\mathrm{T}\circ}/\mathrm{h}$ and $[4 \cdot 9352 \quad 4 \cdot 5242 \quad 4 \cdot 9166]^{\mathrm{T}}$ mg. Moreover, we also deduce that the proposed approach performs better during the steady state from Figure 5 to 8.

5. CONCLUSION. This paper describes the in-motion alignment procedure for a low-cost INS/GPS integrated system under random misalignment angles using the second order extended Kalman filter structure. Based on Rodrigues parameters representation, an alignment model with a linear system equation and second order nonlinear measurement equation is established. The second order extended Kalman filter framework enables the proposed method to estimate the gyroscope and accelerometer biases apart from the initial alignment, which is optimised for low-cost Micro Electro Mechanical System (MEMS)-based SINS.

From the experimental test results, it has been clearly indicated that the proposed alignment approach can achieve the initial alignment more quickly and more accurately compared with the conventional approaches.

REFERENCES

Bimal, R.K. and Ashok, J. (2015). In-motion Alignment of Inertial Navigation System with Doppler Speed Measurements. *AIAA Guidance, Navigation, and Control Conference*, Kissimmee, Florida.

Burak, H.K. and Bekir, S. (2015). In-motion Alignment of a Low-cost GPS/INS under Large Heading Error. *The Journal of Navigation*, **68**, 355–366.

Chang, L.B., Li, J.S. and Chen, S.Y. (2015). Initial alignment by attitude estimation for strapdown inertial navigation systems. *IEEE Transactions on Instrumentation and Measurement*, **64**, 784–794.

Choukronun, D., Bar-Itzhack, I.Y. and Oshman, Y. (2004). Optimal-REQUEST algorithm for attitude determination. *Journal of Guidance, Control, and Dynamic*, **27**, 418–425.

Daniele, M., Markley, F.L. and Puneer, S. (2007). Optimal Linear Attitude Estimator. *Journal of Guidance, Control, and Dynamic*, **30**, 1619–1627.

Dissanayake, G., Sukkarieh, S., Nebot, E.M. and Durrant-Whyte, H. (2001). The Aiding of a Low-Cost Strapdown Inertial Measurement Unit Using Vehicle Model Constraints for Land Vehicle Applications. *IEEE Transactions on Robotics and Automation*, **17**, 731–747.

Gu, G., EI-Sheimy, N. and Hassan, T. (2008). Coarse alignment for marine SINS using gravity in the inertial frame as a reference. *IEEE/ION Position Location and Navigation Symposium, Monterey, California, USA*, 961–965.

Han, S. and Wang, J. (2010). A novel inertial alignment scheme for low-cost INS aided by GPS for land vehicle application. *Journal of Navigation*, **63**, 663–680.

Jamshaid, A. and Muhammad, U. (2009). A consistent and robust Kalman filter design for in-motion alignment of inertial navigation system. *Measurement*, **42**, 577–582.

Joon, G.P., Jang, G.L. and Chan, G.P. (2004). SDINS/GPS in-flight alignment using GPS carrier phase rate. *GPS Solutions*, **8**, 74–81.

Junkins, J.L. and Kim, Y. (1993). Introduction to Dynamics and Control of Flexible Structures, AIAA Education Series, AIAA, Washington, DC.

Kang, T.Z. Fang, J.C and Wang, W.G. (2012). Quaternion-Optimization-Based In-Flight Alignment Approach for Airborne POS. *IEEE Transactions on Instrumentation and Measurement*, **61**, 2916–2923.

Kong, X., Nebot, E.M. and Durrant-Whyte, H. (1999). Development of a Nonlinear Psi-Angle Model for Large Misalignment Errors and Its Application in INS Alignment and Calibration. *Proceedings of the IEEE International Conference on Robotics and Automation*, Detroit, MI.

Li, H., Pan, Q., Wang, X., Jiang, X. and Wang, J. (2015). Kalman filter design for initial precision alignment of a strapdown inertial navigation system on a rocking base. *Journal of Navigation*, **68**, 184–195.

Li, J., Xu, J., Chang, L. and Feng, Z. (2014). An Improved Optimal Method for Initial Alignment. *Journal of Navigation*, **67**, 727–736.

Li, W. and Wang, J. (2013). Effective adaptive Kalman Filter for MEMS- IMU/ Magnetometers Integrated Attitude and Heading Reference Systems. *Journal of Navigation*, **66**, 99–113.

Li, W., Wang, J., Lu, L. and Wu, W. (2013). A novel Scheme for DVL-Aided SINS In-Motion alignment using UKF techniques. *Sensors*, **13**, 1046–1063.

Lu, J., Xie, L. and Li, B. (2016). Applied Quaternion Optimization Method in Transfer Alignment for Airborne AHRS Under Large Misalignment Angle. *IEEE Transactions on Instrumentation and Measurement*, **65**, 346–354.

Mei, C., Qin, Y. and Yang, P. (2015). Linear optimized self-alignment for SINS using Rodrigues parameters. *Journal of Chinese Inertial Technology*, **23**, 298–302.

Qin, Y. (2014). *Inertial Navigation*, Science Press, Beijing, 2nd Ed.

Qin, Y., Zang, H. and Wang, S. (2014). *Kalman filter and integrated navigation theory*, Northwestern Polytechnical University, 3nd Ed.

Savage, P.G. (1998). Strapdown inertial navigation integration algorithm design, Part1: Attitude algorithms. *Journal of Guidance, Control, and Dynamic*, **21**, 19–28.

Scherzinger, B.M. (1996). Inertial Navigation Error Models for Large Heading Uncertainty. *IEEE Proceedings of PLANS*, 447–484.

Shuster, M.D. and Oh, S.D. (1980). Three-Axis Attitude Determination from Vector Observations. *Guidance and Control*, **4**, 70–77.

Silson, P.M.G. (2011). Coarse Alignment of a Ship's Strapdown Inertial attitude reference system Using Velocity Loci. *IEEE Transactions on Instrumentation and Measurement*, **60**, 1930–1941.

Simon, D. (2006). Optimal State Estimation Kalman, H_∞, and Nonlinear Approaches, John Wiley & Sons, Inc., Hoboken, New Jersey.

Wu, M., Wu, Y., Hu, X. and Hu, D. (2011). Optimization-based alignment for inertial navigation systems: Theory and algorithm. *Aerospace science and technology*, **5**, 1–17.

Wu, Y., and Pan, X. (2013). Velocity/Position Integration Formula part I: Application to In-flight Coarse Alignment. *IEEE Transactions on Aerospace and Electronic System*, **49**, 1006–1023.

Yuan, D., Ma, X., Liu, Y and Zhang, C. (2016). Dynamic Inertial Alignment of the MEMS-based Low-cost SINS for AUV based on Unscented Kalman Filter. *OCEANS 2016-Shanghai*. IEEE.